PACKING OPTIMIZATION GUIDELINES

SUMMARY

LIST OF TABLES

LIST OF FIGURES

1 SCOPE

There is an increasing demand from valve end users for low emission sealing systems, but it remains important that the valve continues to move smoothly and efficiently. Since the frictional load of the stem packing has a contrary effect on these two requirements, valve and valve packing manufacturers are challenged with respect to the prediction and improvement of packing behavior in a valve.

The following guideline provides an analytical calculation model for the whole bolting/gland/stuffing box/packing assembly, evaluating the packing load evolution over the different using conditions, including tightening phase and pressurization high-temperature phase. Associated dedicated packing characterization test procedures are also given here in order to asses both packing mechanical and sealing behaviors parameters required for the calculation. This package (calculation + test procedures) enables the user to optimize the initial packing tightening force of the gland in order to fulfil required sealing performances while lowering as much as possible the induced packing/stem friction.

These guidelines have been developed in collaboration with ESA (European Sealing Association), FSA (Fluid Sealing Association) and the Fluid Equipment Committee of CETIM (composed of French valve and sealing product manufacturers) who has initiated the work program.

2 NOMENCLATURE

Indices

- S : Stem
- SB : Stuffing Box
- G : Gland
- FG : Gland flange
- P : Packing
- I : Situation number (assembly =0) I=1,2,…
- k : Ring number k=1,2,…n in the stack (numbered from the gland)
- k_{seal} : Greatest value of k for which a tightness requirement is defined
- LL : Live-Loading system

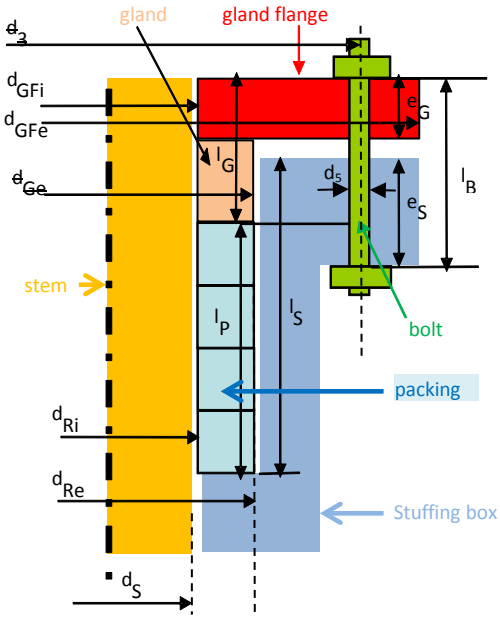

Figure 1: Packing system sketch

Variables

- A_B : Total bolt section [mm²]
- A_P : Compressed rings surface area ($A_P = \pi/4 * (d^2_{Re} - d^2_{Ri})$) [mm²]
- b_{GF} : Ring flange effective width [mm]
- d_3, d_{3e} : Bolt circle diameter real, effective [mm]
- d_5, d_{5e} : Bolt hole diameter real, effective [mm]
- d_7 : Diameter of position of reaction between gland flange and gland, assumed to be positioned in the middle of contact area between gland flange and gland [mm]
- d_B : Bolt diameter [mm]
- d_{Ge} : Gland external diameter [mm]
- d_{GFi}, d_{GFe} : Internal and external gland flange diameters [mm]
- d_{Ri}, d_{Re} : Internal diameter (stem side) and external diameter (stuffing box side) of the ring (considered identical for the whole packing) [mm]
- d_S : Stem diameter [mm]

- $e_{Rk,I}$: Thickness of ring k, in the situation I [mm]
- e_{SB} : Stuffing box flange ring thickness [mm]
- e_{GF} : Gland flange ring thickness [mm]
- e_P : Compressed packing ring thickness [mm]
- $f_{B,I}$, $f_{GF,I}$: Nominal design stresses for the bolt, the gland flange [mm]
- $E_{Pk,I}$: Young modulus of the ring k, at the temperature I [MPa]
- E_R : Packing ring unloading elastic modulus [MPa]
- $F_{B0min;}$ $F_{B0nom;}$ F_{B0max} : Minimal, nominal, maximal bolt load in assembly situation given the tightening method dispersion [N]
- $F_{B0,Ireq,}$: Bolt load required in assembly situation (situation 0) to check the tightness requirement in the situation I (I ≥1) [N]
- $F_{BI,Ireq,}$: Bolt load required, in the situation I, to fulfill tightness in the situation I [N]
- $F_{B0,allreq}$: Bolt load required in situation 0 to fulfill tightness in all the situations [N]
- F_{Fa}, F_{Fr} : Dynamic friction effort (axial for translation movement, radial for rotation movement) between the stem and the packing [N]
- $F_{LLmax,I}$: Force corresponding to the maximum live-loading system deflection [N]
- F_{motor} : Maximum force of the actuator motor [N]
- $F_{P,I}$: Axial effort due to the end thrust effect [N]
- $F_{Rk,I}$: Axial force applied on upper face of the ring k in the situation I [N]
- $K_{k,I}$: Radial transmission coefficient (considered identical for the stem and the stuffing box interfaces) of force for the ring k in the situation I [N/mm]
- K : Transmission coefficient of stress from axial to radial direction (considering the axial stress applied on packing ring upper face as a reference). This parameter is considered identical for the stem and the stuffing box interfaces [-]
- K' : Transmission coefficient of stress from axial to radial direction (considering the average of axial stress applied on packing ring upper and bottom face as a reference). This parameter is considered identical for the stem and the stuffing box interfaces [-]
- $K_{LL,I}$: Live-loading system stiffness [N/mm]
- $K_{P+LL,I}$: Stiffness of serial association of live-loading system and packing [N/mm]
- l_B : Initial bolt length between nuts/bolt head with uncompressed packing [mm]
- l_{Bcomp} : Bolt distance between nuts/bolt head with compressed packing (condition 0 – tightening) [mm]
- $l_{SB,}$: Axial distance from the bottom and the top face of the stuffing box [mm]

- l_G : Axial distance from the gland (or gland flange) top face (in contact with the bolts) and bottom face (in contact with the first ring) [mm]
- l_{LL} : Live-loading system height (with no tightening and at room temperature) [mm]
- n_B : Number of bolts [-]
- n : Number of packing rings [-]
- P_I : Fluid pressure in the situation I [MPa]
- $Q_{A(L)}$: Minimum required axial surface pressure on the ring in the assembly situation, which is necessary for the validity of $Q_{smin(L),I}$ in operating conditions [MPa]
- Qaxial,sup, Qaxial,inf : Axial contact pressure (coming from the axial load applied by the gland) on the upper, lower packing ring face[MPa]
- Qradial : Radial contact pressure on the packing ring at stuffing-box interface [MPa]
- QAX, Q: Axial contact pressure applied by the gland on the upper packing ring face during the test in initial step, in the current test phase [MPa]
- $Q_{smin(L)}$: Minimum required level of residual axial surface pressure on the ring for the tightening class L in pressurized situation [MPa]
- $Q_{min(L)}$: Minimum required level of axial surface pressure on the ring for the tightening class L in assembly situation (lowest value accepted for $Q_{A(L)}$) [MPa]
- $R_{RSk,I}$, $R_{RSBk,I}$: Radial force applied by the ring k in the situation I on the stem and on the stuffing box respectively [N]
- $Rx_{k,I}$: Relaxation coefficient of the ring k in the situation I, giving the ratio of residual to initial force measured during a pure relaxation test [-]
- Rx_I Mean value of the whole packing relaxation coefficients in the situation I [-]
- Tamb : Laboratory room temperature during the test
- T : Applied temperature during the test
- T_0: Initial temperature (T_0) assumed to be homogeneous for all the elements [°C]
- $T_{B,I}$, $T_{SB,I}$, $T_{P,I}$, $T_{G,I}$: Temperature of the different elements in situation I [°C]
- T_{motor} : Maximum torque for the actuator motor [N.mm]
- Tf : Torque measured on the valve stem due to packing friction during stem movement [N.m]
- $\alpha_{B,I}$, $\alpha_{SB,I}$, $\alpha_{Rk,I}$, $\alpha_{G,I}$: Thermal expansion coefficient for the considered element , between the assembly temperature (situation 0) and the situation I [K^{-1}]
- $\Delta e_{Pcreep\ k,I}$: Deflection variation over time of ring number k, due to creep phenomena [mm]

- ΔU^{T}_{I} : Variation of the available height for the packing between assembly phase and situation I, due to thermal expansion [mm]
- ΔU^{M}_{I} : Variation of available height for the packing between assembly phase and situation I due to packing creep/relaxation, ($\Delta U^{M}_{I} \leq 0$) [mm]
- ΔF^{T}_{I} : Variation of the axial force applied on the packing between assembly phase and situation I, due to thermal expansion [N]
- ΔF^{M}_{I} : Variation of the axial force applied on the packing between assembly phase and situation I, due to packing creep/relaxation ($\Delta F^{M}_{I} \leq 0$) [N]
- ε^{-}, ε^{+} : Tightening dispersion coefficients [-]
- Φ_{B}, $\Phi_{GF,}$ Φ_{F} : Load ratio for the bolt, the gland flange and the friction respectively [-]
- $\mu_{Sk,I}$, $\mu_{SBk,I}$: Static friction force coefficients (respectively stem side and stuffing box side) for the ring k in the situation I [-]
- μS,μSB : Packing ring static friction force coefficients at stem interface, at stuffing box interface) [-]
- μ_{ftrans}, μ_{frot} : Dynamic friction coefficient, translation, rotation movement, between the stem and the ring [-]

3 MECHANICAL MODEL DESCRIPTION

3.1 Outlines and hypothesis of the mechanical model

Each ring is characterized individually. The possible interaction between the rings in the stack is not taken into account. Diany and Bouzid [14] observed that the evolution of the radial contact pressure (directly linked to the sealing level and the friction at its interface) according to the axial position does not depend on the number of rings in the stack. The stem movements are systematically carried out before pressurization of the valve, involving load homogenization within the packing. The gland deformations (bending) are neglected. The axial bolt load is considered to be fully transferred to the first ring in contact with the gland and no alignment problem is taken into account. The gland is considered having a purely axial displacement. The mechanical model accounts for deformation and stiffness of the packing and the live loading-system. The other components as gland, stuffing box or bolts are considered to have an infinite rigidity.

The ring properties values (K, μ…) are considered to be constants within each ring (no variation depending on the axial position in the ring). The calculation method enables to differentiate the packing ring static friction coefficients on the stem side and the stuffing box side (μ_S and μ_{SB}). Nevertheless, in a first approach $\mu_S = \mu_{SB}$ is assumed with μ_{SB} measured during the tests.

The pressure end thrust is considered in two different ways in the calculation procedure.

- For the calculation of the required bolt load in assembly situation to check the tightness criteria, the fluid pressure is assumed to reach the bottom face of the gland, simulating a full migration of the fluid through the packing up to the upper face of the ring in contact with the gland. This approach, by lowering the axial load on the rings, is conservative in this calculation phase. The end thrust effect is subtracted to the bolt force to obtain the axial force applied on the first packing ring.
- For the integrity check, the fluid is considered to apply an additional axial compressive force on the bottom face of the packing bottom ring. A full axial transfer of this additional force through the packing is assumed. Thus, the end thrust effect is added to the bolt force to obtain the axial force applied on the first packing ring.

The packing creep/relaxation behavior is handled in two different ways depending on the presence (or not) of a live loading system.

- When no live-loading system is installed or if the live loading-system is not effective, the packing housing is considered to be rigid and a pure relaxation phenomenon is considered for the packing material.
- When a live-loading system is installed (and is active), the additional ring deflection due to creep ($\Delta_{ePcreep\ k,l}$), measured during pure creep test (constant load on the ring) is considered. Then the force variation on the packing due to packing creep ($\Delta F^{M}_{l} \leq 0$) is calculated considering the live loading system rigidity.

The proposed method is considering that the variations involved by the thermal expansions are occurring before the creep/relaxation packing phenomena, (linked to the packing material own response time).

3.2 Packing parameters involved in the model

The major characteristics defining the packing rings behavior are:

- For sealing behavior: the required axial contact pressure at tightening $Q_{A(L)}$ and during operation $Q_{smin(L)}$ to meet the tightness class L.
- For mechanical behavior:
  - Rx or Δe_{Pcreep} : the relaxation (or creep) coefficient
  - K: the axial to radial load transmission coefficient
  - μ_f: the dynamic friction coefficient at stem/packing interface (under stem translation or rotation)

The method also enables to handle second order parameters for possible deeper modelling as:

- The static friction coefficient at stem/packing and housing/packing interface
- The elastic modulus of the ring at unloading
- The rings load/thickness curve
- The ring axial thermal expansion

3.3 Principle

The method involves two major steps as described in Figure 2 and Figure 3.

1. Calculation of the required initial bolt load to fulfil the tightness criteria in all the situations (assembly and operations) and definition of the tightening range from the tool dispersion
2. Check the mechanical integrity of the bolt and the gland flange and check of packing friction level for an initial bolt force corresponding to the upper bound of the tightening range

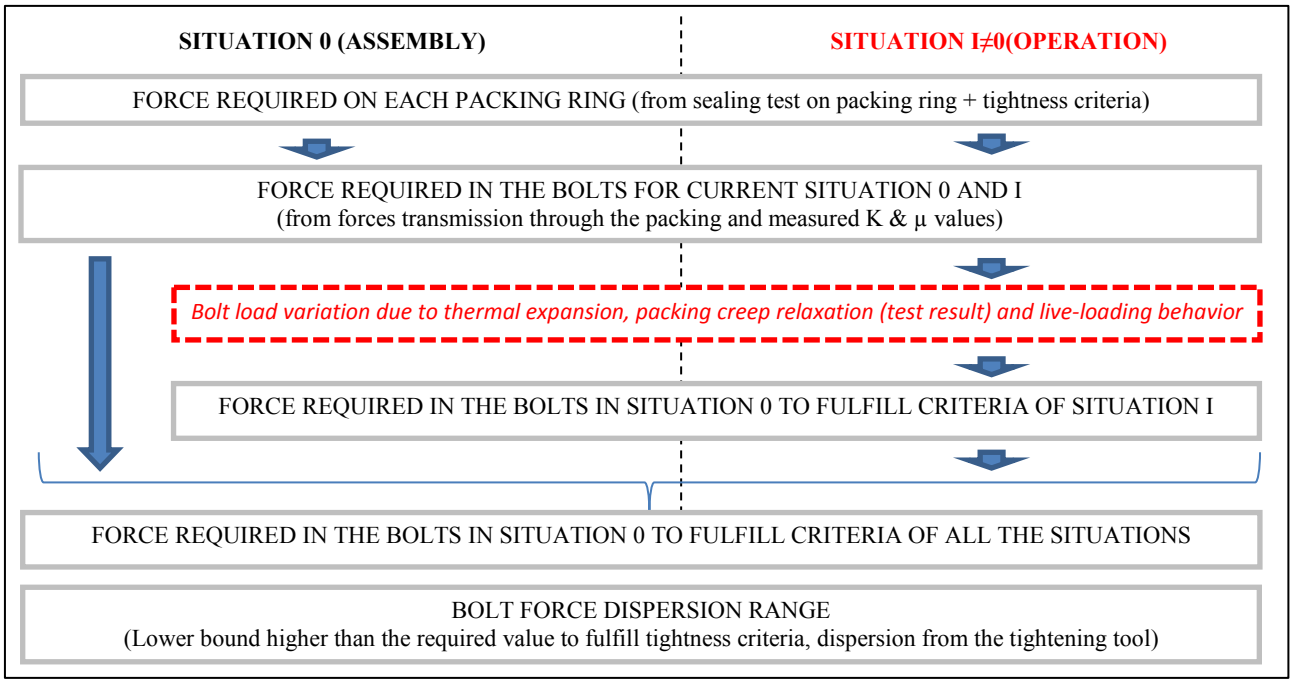

Figure 2- Calculation of the required initial bolt load

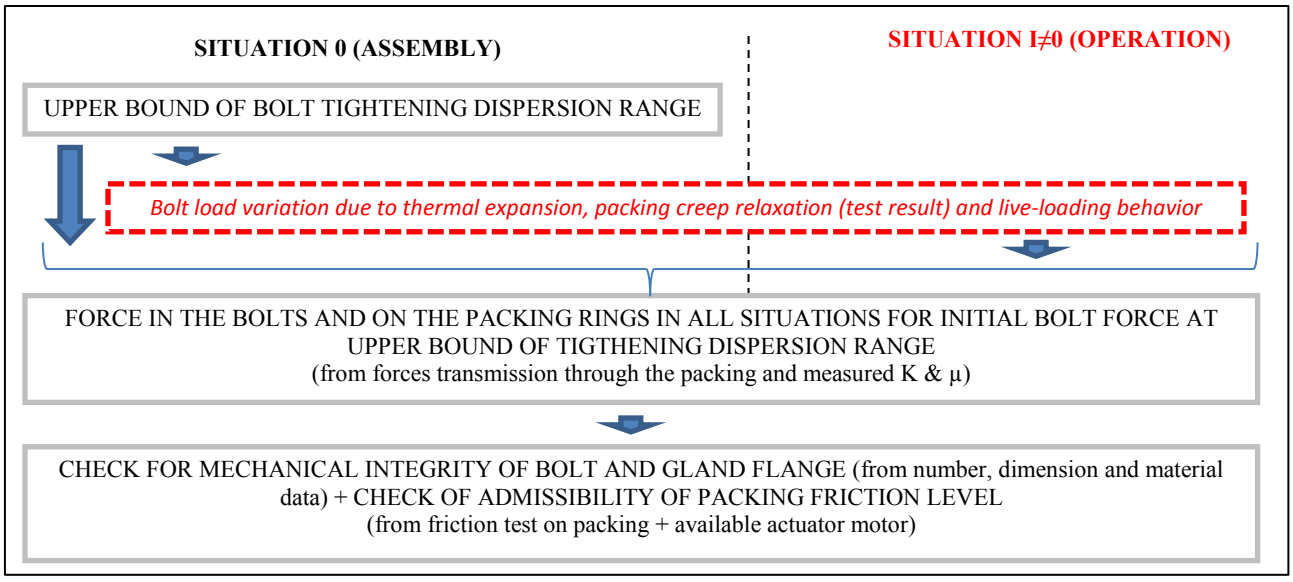

Figure 3- Check of mechanical integrity

3.4 Calculation of the required initial bolt load for tightness criteria in all situations

3.4.1 Required bolt load in situation I to fulfill criteria of the current situation I (including I=0)

By assumption, the force applied by the bolts to the gland is completely transmitted to the upper face of the first ring (k=1). For the pressurized situations, it is considered that the fluid involves a force applying on the gland.

$$F_{R1,I} = F_{BI,I} - F_{P,I} \tag{1}$$

From [11], the transmission of axial force on ring number k, from the upper face to the bottom face is defined by the following equation, assuming that K and μ factors are homogeneous in the ring number k.

$$F_{Rk+1,I} = F_{Rk,I} \times \exp\left(\left[-4 \times K_{k,I} \times \frac{\mu_{Sk,I} \times d_{Ri} + \mu_{SBk,I} \times d_{\mathrm{Re}}}{d_{\mathrm{Re}}^{\ 2} - d_{Ri}^{\ 2}}\right] \times \left(e_{Pk,I}\right)\right) \tag{2}$$

Step by step, the axial force applied on the ring k is thus related to the axial force applied on the ring number 1, in contact with the gland.

$$F_{Rk,I} = F_{R1,I} \times \exp\left(-4 \times \sum_{i=1}^{k-1} K_{i,I} \times \frac{\mu_{Si,I} \times d_{Ri} + \mu_{SBi,I} \times d_{\mathrm{Re}}}{d_{\mathrm{Re}}^{\ 2} - d_{Ri}^{\ 2}} \times e_{Pi,I}\right) \tag{3}$$

1 From equation above, the axial force applied on the ring decreases with the distance to the gland. As the sealing function is not necessarily required for all the rings (for example anti-extrusion rings), the definition of k_{seal}, is introduced as the highest value of k for which a sealing function is required. The following relations must then been verified:

If I=0
$$F_{Rkseal,0} \geq MAX(Q_{\min(L)}; Q_{A(L)}) \times A_P \tag{4}$$

If I≠0
$$F_{Rkseal,I} \geq Q_{s\min(L)} \times A_P \tag{5}$$

The lowest value of $F_{BI,I}$ in (1) enabling to fulfill (4) and (5) is defined as $F_{BI,Ireq}$

3.4.2 Required bolt load in situation 0 to fulfill criteria of the situation I (I≠0)

3.4.2.1 Thermal expansion

The axial thermal expansions are calculated from the assembly situation (uniform temperature T_0 in the whole assembly), using equation (6), which assumes that the temperature is uniform among the whole assembly. When ΔU^T_I >0 (respectively <0), the thermal expansion tends to increase (respectively decrease) the available length for the packing and the live-loading system (see Figure 4)

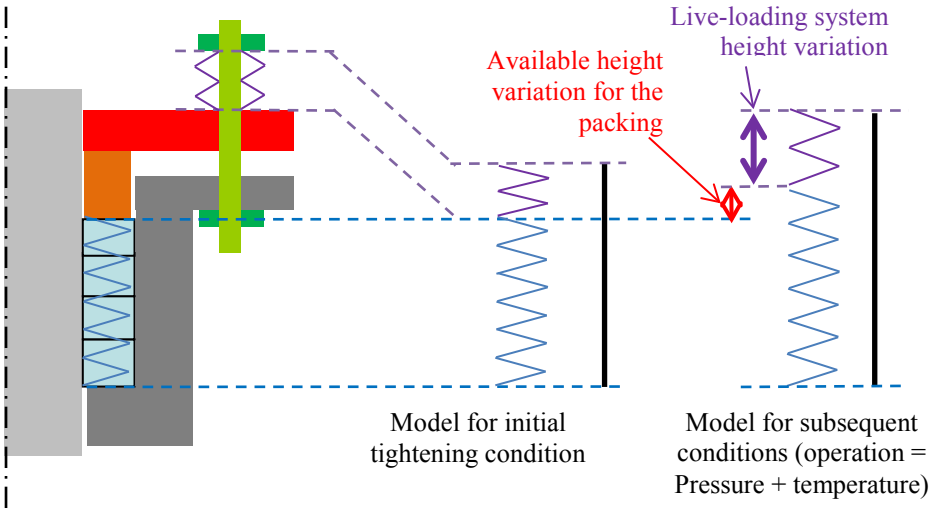

Figure 4- Thermal expansion

$$\Delta U^T{}_I = (l_{B_{comp}} - l_{LL}) \times \alpha_{B,I} \times (T_{B,I} - T_0) + (l_{SB} - e_{SB}) \times \alpha_{SB,I} \times (T_{SB,I} - T_0) - \left(\sum_{i=k}^{n} (e_{Rk,I} \times \alpha_{Rk,I}) \right) \times (T_{P,I} - T_0) - l_G \times \alpha_{G,I} \times (T_{G,I} - T_0) \quad (6)$$

The live-loading system is assumed to have a constant rigidity (K_{LL}) for applied force lower than $F_{LLmax,I}$ (system ON) and an infinite rigidity for higher loads (system OFF). Thus, depending on the bolt load level applied, the rigidity of the serial combination made by the packing and the live-loading system (K_{P+LL}) will differ (ON/OFF) as shown in equations (7) and (8).

$$K_{P+LL,I}(ON) = \frac{1}{\sum_{i=1}^{n} \frac{1}{E_{Pi,I} \times A_P / e_{Pi,I}} + \frac{1}{K_{LL,I}}} \quad (7)$$

$$K_{P+LL,I}(OFF) = \frac{1}{\sum_{i=1}^{n} \frac{1}{E_{Pi,I} \times A_P / e_{Pi,I}}} \quad (8)$$

The force variation between situation 0 and I, due to thermal expansion is then calculated using equation (9). The case where the live-loading system is not always active (live-loading in end position at initial tightening but being as soon as the bolt force decrease in the service situation) is also considered using a combination of K_{P+LL}(ON) and K_{P+LL}(OFF).

$$\Delta F^{T}{}_{I} = -K_{P+LL,I} \times \Delta U^{T}{}_{I} \tag{9}$$

The live-loading system behavior is divided in two phases, depending on the force applied on it:

- Applied force < $F_{LLmax,I}$: system working (ON) and rigidity equal to $K_{LL,I}$
- Applied force > $F_{LLmax,I}$: system not working (OFF) and rigidity considered infinite regarding the packing rigidity

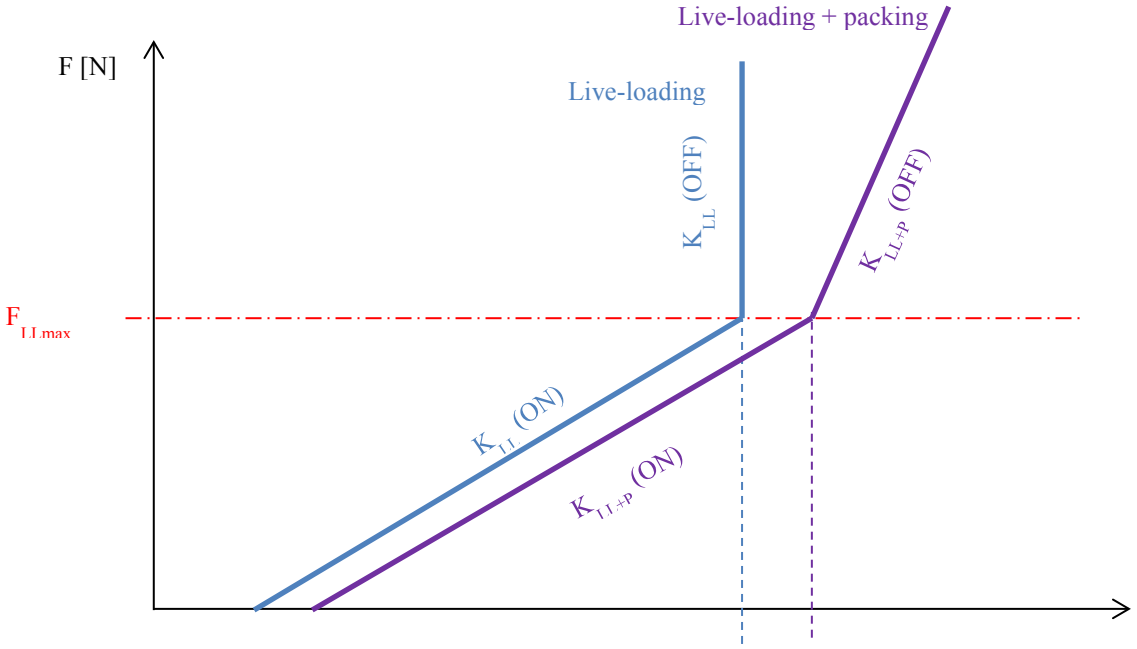

Figure 5: Live-loading and live-loading+packing combination behavior diagram

Table 1 gives the different behavior types of the live-loading system depending on the relative position of $F_{BI,I}$-$\Delta F^{T}{}_{I}$, $F_{BI,I}$ and $F_{LLmax,I}$.

Table 1 : Live loading behavior depending on bolt load relative values.

1	$F_{BI,I} \leq F_{BI,I}-\Delta F^{T}{}_{I}(ON) \leq F_{LLmax,I}$ Figure 6	$\Delta F^{T}{}_{I} = \Delta F^{T}{}_{I}(ON)$	**(10)**
2	$F_{BI,I}-\Delta F^{T}{}_{I}(ON) \leq F_{BI,I} \leq F_{LLmax,I}$ Figure 7		
3	$F_{BI,I} \leq F_{LLmax} \leq F_{BI,I}-\Delta F^{T}{}_{I}(ON)$ Figure 8	$\Delta F^{T}{}_{I} = F_{BI,I} - F_{LL\max,I} - K_{P+LL,I}(OFF) \times \left[\Delta U^{T}{}_{I} + \frac{F_{BI,I} - F_{LL\max,I}}{K_{P+LL,I}(ON)} \right]$	**(11)**
4	$F_{LLmax,I} \leq F_{BI,I} \leq F_{BI,I}-\Delta F^{T}{}_{I}(ON)$ Figure 9	$\Delta F^{T}{}_{I} = \Delta F^{T}{}_{I}(OFF)$	**(12)**
5	$F_{LLmax,I} \leq F_{BI,I}-\Delta F^{T}{}_{I}(ON) \leq F_{BI,I}$ Figure 10		
6	$F_{BI,I}-\Delta F^{T}{}_{I}(ON) \leq F_{LLmax,I} \leq F_{BI,I}$ Figure 11	$\Delta F^{T}{}_{I} = F_{BI,I} - F_{LL\max,I} - K_{P+LL,I}(ON) \times \left[\Delta U^{T}{}_{I} + \frac{F_{BI,I} - F_{LL\max,I}}{K_{P+LL,I}(OFF)} \right]$	**(13)**

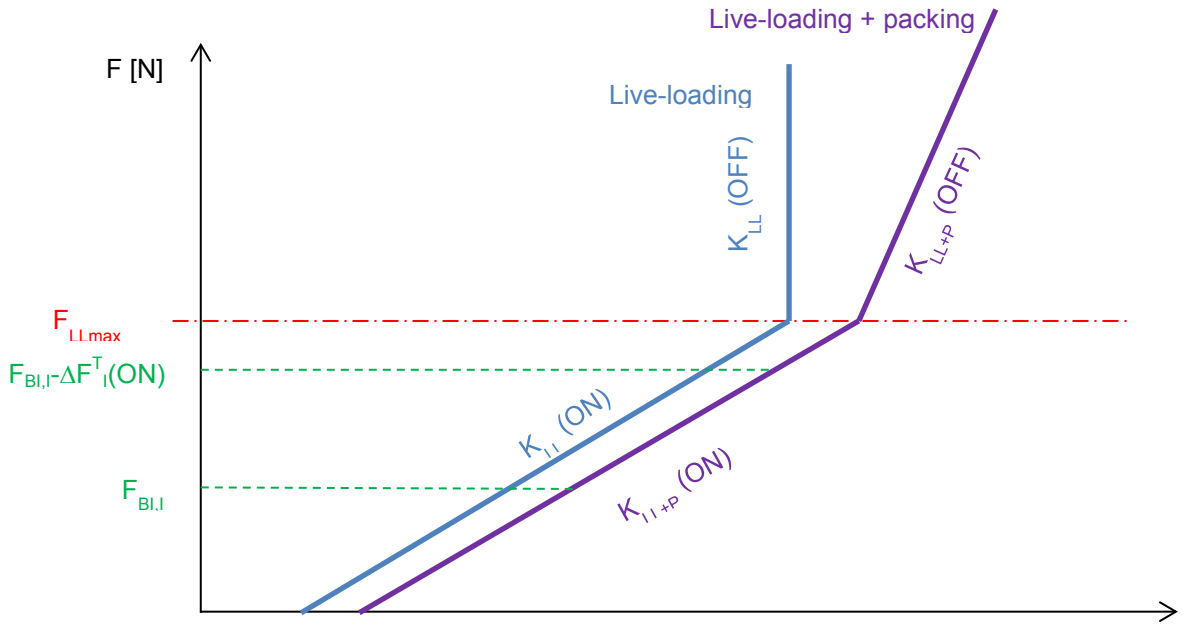

Figure 6: live-loading+packing combination behavior diagram (case1)

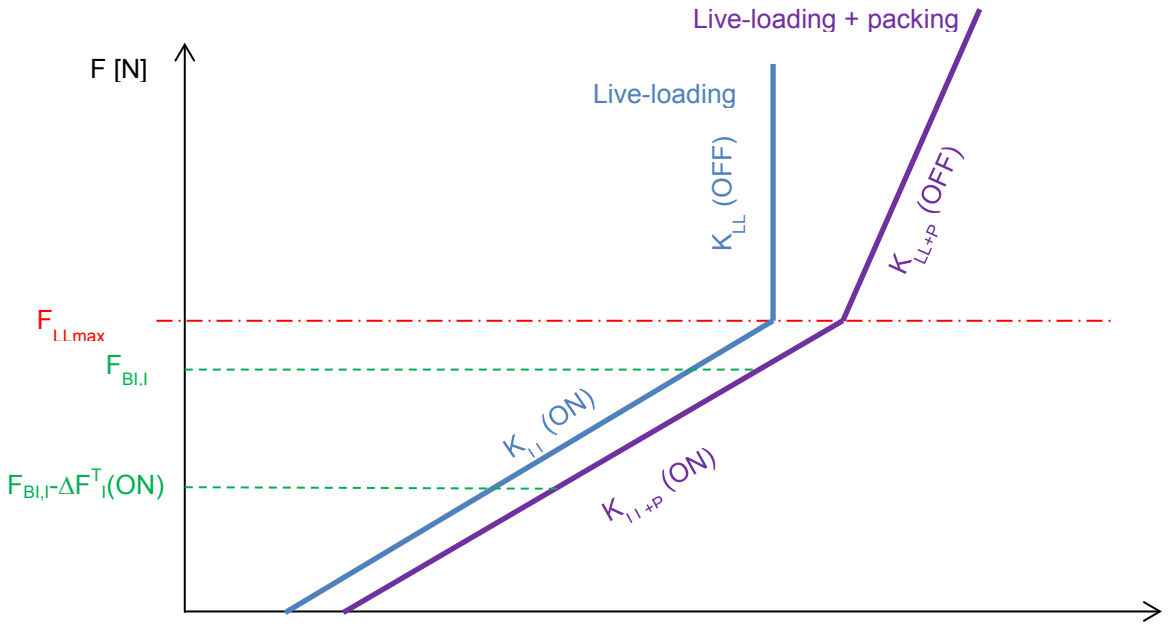

Figure 7: live-loading+packing combination behavior diagram (case2)

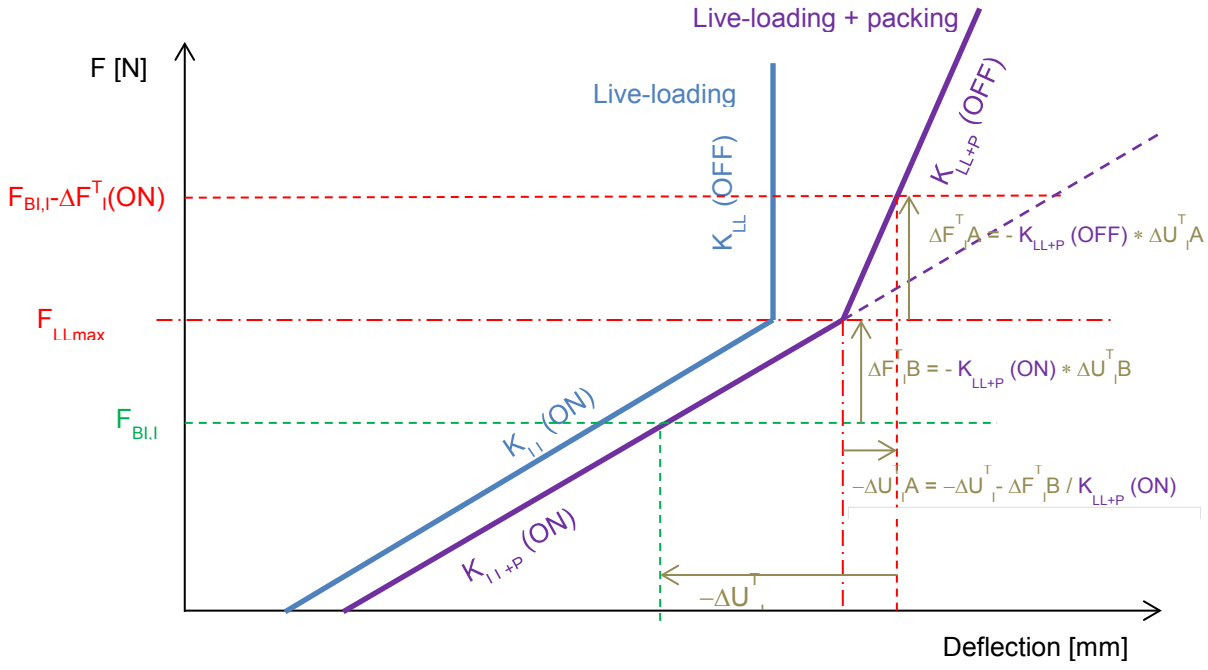

Figure 8: live-loading+packing combination behavior diagram (case3)

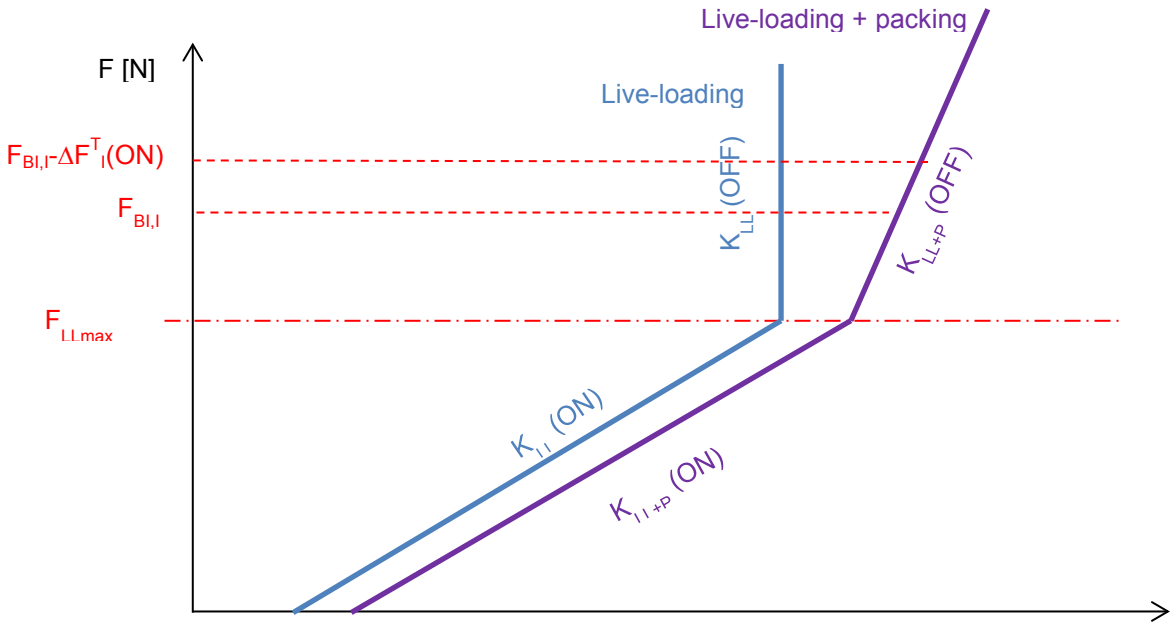

Figure 9: live-loading+packing combination behavior diagram (case4)

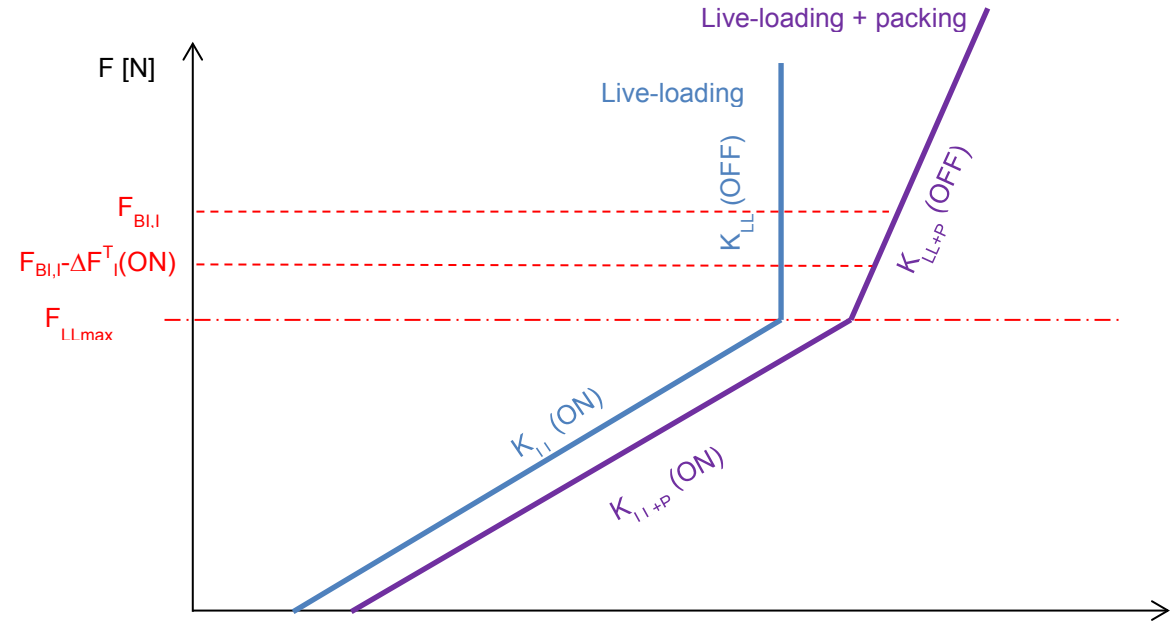

Figure 10: live-loading+packing combination behavior diagram (case5)

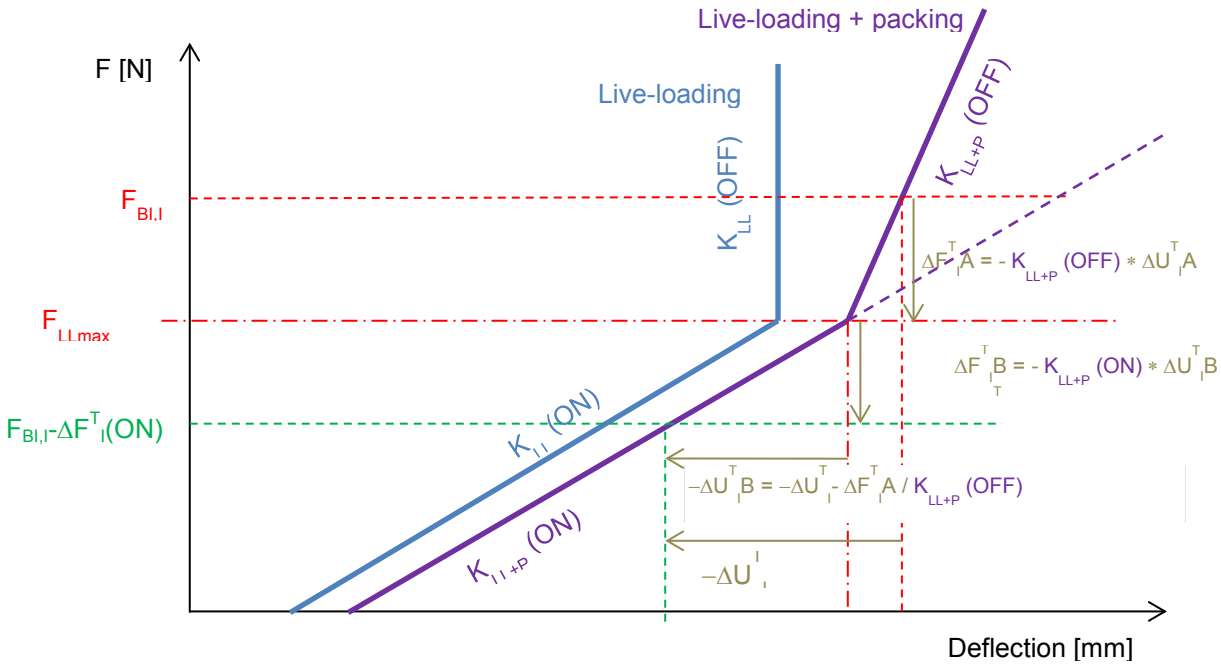

Figure 11: live-loading+packing combination behavior diagram (case6)

3.4.2.2 *Packing creep relaxation*

As described in the mechanical model section, when no live-loading is installed or if the live loading is not operational, the approach of a pure relaxation behavior (no variation of the packing housing) is considered and the force variation between situation 0 and situation I due to packing relaxation ($\Delta F^M_I<0$), is calculated using equations (14) and (11). For simplification, a global value of the relaxation coefficient Rx is calculated for the whole packing in (15), as an arithmetic average of the various Rx_k values obtained for the different rings of the packing.

$$Rx_I = 1/n \times \sum_{k=1}^{n} Rx_{k,I} \qquad (14)$$

$$\Delta F_{req}{}^M{}_I = (1 - \frac{1}{Rx_I}) \times F_{BI,I} \leq 0 \qquad (15)$$

When a live-loading is installed and operational, a creep/relaxation for a stiffness corresponding to the live-loading system should theoretically be performed. Nevertheless, regarding the huge number of testing configuration involved this approach is not considered. It is then proposed do perform pure creep test (stiffness equal to zero), by measuring the additional ring deflection due to creep ($\Delta e_{Pcreep\ k,I}$) while maintaining a constant force on the ring. This approach tends to

maximize the additional ring deflection due to creep by maintaining the load on the ring at a higher level than for the real system (on site). Global packing set thickness variation due to creep is defined by (16) and associated force variation is calculated by (17) considering the live-loading system rigidity corresponding to the load range applied on it.

$$\Delta U^{M}{}_{I} = \sum_{k=1}^{n} \Delta e_{Pcreep\,k,I} \geq 0 \quad (16)$$

$$\Delta F^{M}{}_{I} = -K_{LL,I} \times \Delta U^{M}{}_{I} \leq 0 \quad (17)$$

3.4.3 Initial required bolt force to fulfill situation I criteria

The initial bolt force $F_{B0,Ireq}$ required in assembly situation (situation 0) in order to get the minimum required bolt force in the situation I is given by equation (18).

$$F_{B0,I_{req}} = F_{BI,I_{req}} - \Delta F_{req}{}^{T}{}_{I} - \Delta F_{req}{}^{M}{}_{I} \quad (18)$$

3.4.4 Required bolt load in situation 0 to fulfill criteria of all the situations

In order to check tightness requirement in all situations, the maximum value of the initial bolt load required in the assembly situation to check tightness requirement of each situation I is calculated.

$$F_{B0,\text{all req}} = \underset{I}{MAX}(F_{B0,\text{I req}}) \quad (19)$$

3.4.5 Tightening range definition

Depending on the tightening tool dispersion, the tightening range is defined. The lower bound must be higher than the minimum value required in order to fulfill the tightness criteria.

$$F_{B0,all_{req}} \leq F_{B0\min} = F_{BO_{nom}} \times \left(1-\varepsilon^{-}\right) \leq F_{B0\max} \leq F_{B0\max} = F_{BO_{nom}} \times \left(1+\varepsilon^{+}\right) \quad (20)$$

3.5 Check of mechanical integrity

3.5.1 Calculation of internal forces in situation I (I≠0) for initial tightening at F_{B0max}

$F_{BImax,}$ the bolt load in situation I for the initial tightening load $F_{B0max,}$ is determined using equation (21) by using the method defined before, for the determination of $\Delta F_{req}{}^{T}{}_{I}$ and $\Delta F_{req}{}^{M}{}_{I}$, in order to calculate the values of $\Delta F_{max}{}^{T}{}_{I}$ and $\Delta F_{max}{}^{M}{}_{I.}$. The corresponding force applied on the first ring is calculated by equation (22) assuming that the pressure effect involves an additional force on the packing. The force applied on each ring is then calculated using equation (3) with updated values of packing parameters and packing loads.

$$F_{BI\max} = F_{B0\max} + \Delta F_{\max}{}^{T}{}_{I} + \Delta F_{\max}{}^{M}{}_{I} \quad (21)$$

$$F_{R1,I\max} = F_{BI\max} + F_{P,I} \quad (22)$$

3.5.2 Mechanical integrity check for all the situations with an initial bolt load F_{B0max}

For each situation, load ratios are calculated to check the system integrity. Bolt mechanical integrity is checked using equation (23)

$$\Phi_{\mathrm{BI}} = \frac{\mathrm{F_{BImax}}}{\mathrm{f_{BI}} \times \mathrm{A_B}} < 1 \quad (23)$$

Gland flange mechanical integrity is checked using the approach of EN12516-2 [21] (clause 10.3) for oval flanges with 2 bolts. For circular flanges made of at least 4 bolts, the approach of EN1591-1 [1] for loose flanges is used. The ability of the actuator to move the stem is checked. The axial (respectively radial) friction force involved by each ring is first calculated using equation (2424) from [18] for translation stem movement (respectively equation (25) for rotational stem movement). Then the load ratios are calculated using equation (27) to (29) depending on the stem movement type.

$$F_{Fa\,k,I} = \mu_{f_{trans}k,I}\sigma_{Bk,I}K_{k,I}\pi d_s e_{Pk,I} \quad (24)$$

$$F_{Fr\,k,I} = \mu_{f_{rot}k,I}\sigma_{Bk,I}K_{k,I}\pi d_s e_{Pk,I} \quad (25)$$

$$\sigma_{Bk} = \frac{1}{2} \times (Q_{k,I} + Q_{k+1,I}) \quad (26)$$

Translation	$F_{FaI} = \sum_k F_{Fa\,k,I}$ (27)		$\Phi_{FI} = \frac{F_{Fa\,I}}{F_{motor}}$ (28)

Rotation	$F_{Fr\,I} = \sum_k F_{Fr\,k,I}$ (29)	$T_{FI} = \frac{d_S}{2} \times F_{Fr\,I}$ (30)	$\Phi_{FI} = \frac{T_{FI}}{T_{motor}}$ (31)

4 PACKING CHARACTERIZATION

4.1 TEST RIGS

The test protocols aim at characterizing the packing rings mechanical behaviour and sealing performances.

4.1.1 Structure of the test bench

The test bench is made of the following elements (Figure 12):

- A stem actuator (rotation or linear)
- A test cell in which the packing is positioned (two test cells have been developed: sealing test cell and mechanical test cell)
- A system for friction measurement on the stem during its movement (force transducer for linear movement or torque-meter for rotation movement)
- A compression press applying the desired force sequence to the packing through the gland.

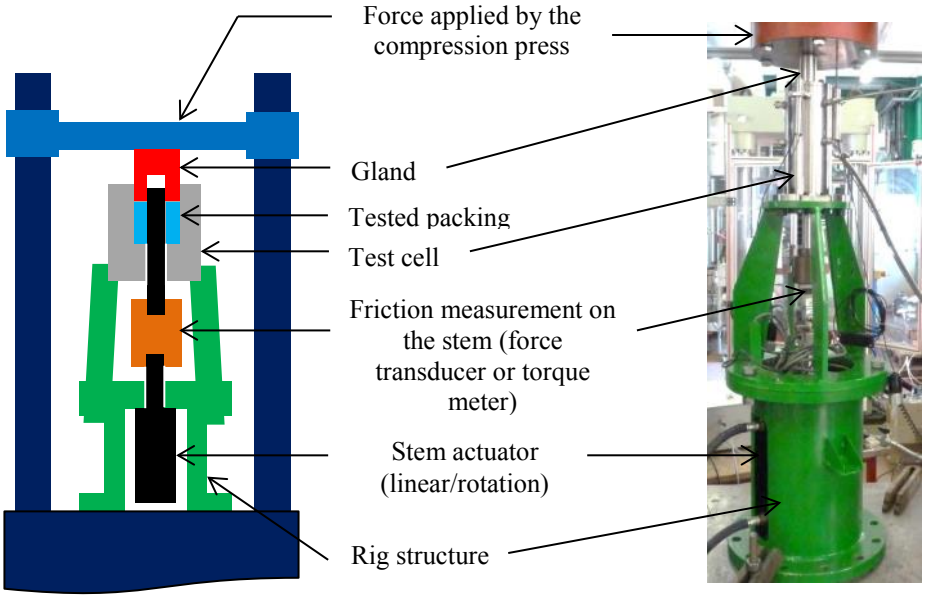

Figure 12: Test rig principle

4.1.2 *The sealing test cell*

The sealing test cell (Figure 13) follows the geometrical characteristics (dimensions, tolerances, surface condition, etc.) of the test rig defined in [3], based on a 4" valve (stem diameter 1 "= 25.4 mm). The tested packing rings should have an internal diameter of 25.4 mm and an external diameter of 38.1 mm. The test cell allows the testing of one to 6 rings (6.35 mm thick each) with a maximum tightening stress of 80 MPa and a maximum helium pressure of 80 bar. The leakage measurement is carried out by helium spectrometry.

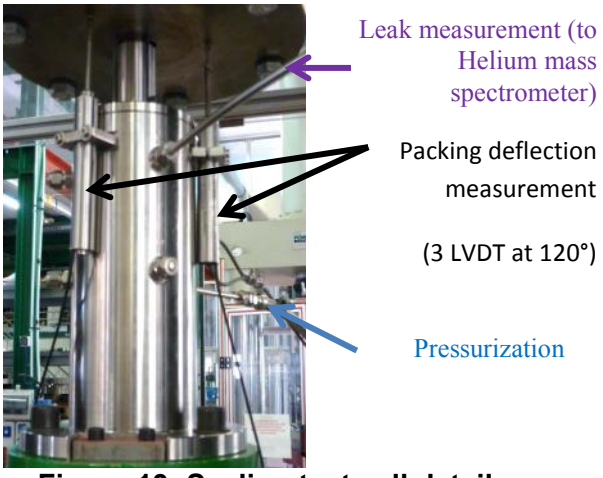

Figure 13: Sealing test cell details

4.1.3 *The mechanical test cell*

The mechanical test cell allows measuring the following quantities:

- The packing rings deflection
- The deformation of the stuffing-box external diameter at packing rings location
- The level of axial force transmitted on the lower (opposed to the gland) face of the packing ring
- The force or torque in the stem during its movement.

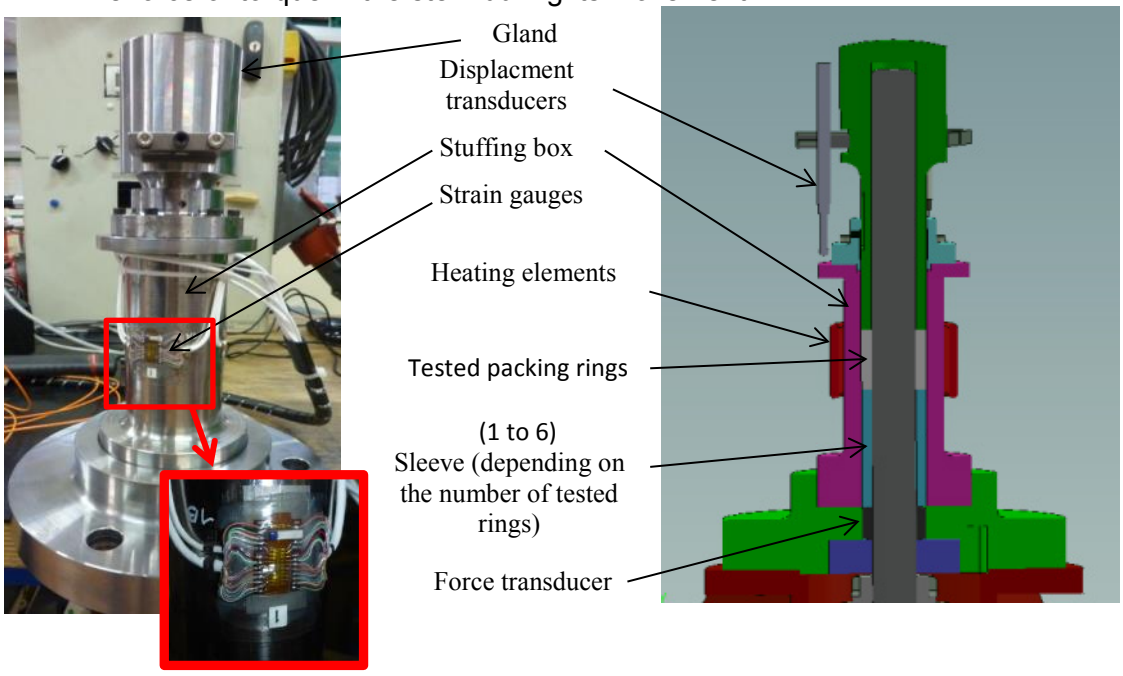

Figure 14: Mechanical test cell details

This cell also follows the dimensional characteristics and the tolerances defined in [3]. The measurement of the deformation on the outside diameter of the housing is carried out using

three 10 gauge chains, angularly positioned at 120 ° in order to check the correct axi-symmetry of the measurements (alignment). This measurement allows determining the contact pressure applied by the packing ring on the inside diameter of the housing through a transfer function determined by finite element analysis.

The thickness of the stuffing-box wall was calculated to provide a deformation level sufficient for the sensitivity of the strain gauges. In the other hand, the wall thickness was selected in order that its deformation does not involve a too high increase of available volume for the packing (not representative of a real valve stuffing box) and ensures its mechanical integrity up to 200°C. The selected wall thickness enables to get enough strain gauge signal with worst case calculated deformation 10 times lower than the acceptable tolerances for the internal diameter of stuffing box given in [3]. The finite element calculations also validated the linearity of the transfer function with respect to the level of contact pressure applied to the internal wall of the housing and the height of the packing under compression.

From the deformation level of the housing outer diameter and the packing ring compressed thickness (measured by the displacement sensors), it is thus possible to determine the level of contact pressure applied by the packing ring on the housing internal diameter. It was validated that the application of the methodology on an elastomeric ring, considered to be incompressible, was correctly inducing a radial contact pressure equal to the axial contact pressure on the investigated stress range.

4.2 TEST PROTOCOLS

4.2.1 Sealing test protocol

The leakage tests aim at establishing the link between the level of contact pressure applied by the gland and the level of sealing obtained, for the considered configuration (number of rings and internal fluid pressure). The procedure reproduces the applied load sequence on the packing by integrating the following steps:

1. Application of the initial stress, Q_A, on upper face ring
2. Application of stem movement (linear or rotation) for stress homogenization within the packing stack while maintaining Q_A,
3. Connection of the helium mass spectrometer
4. Pressurization with Helium at the test pressure (this pressure will be maintained throughout the test)
5. Leakage measurement over 2 hours
6. Unloading to a stress level $Q < Q_A$ with leakage measurement (this step can be repeated several times)

4.2.2 Mechanical Test Protocols

4.2.2.1 Test Protocol1

The first mechanical test protocol aims at determining the following characteristics:

- The packing thickness under the different levels of axial load applied by the gland (e_P)
- The lateral coefficient K (see Figure 15 and 32). This coefficient is assumed to be identical for the radial transmission on the stem and on the stuffing-box side.
- The dynamic friction coefficient at stem/packing interface (μ_{f_rot})
- The coefficient of static friction at the stuffing-box/packing interface (μ_{SB}) (see Figure 15 and 33). This coefficient is assumed to be identical to the coefficient of friction μ_S at the stem/packing interface.

$$K = \frac{Q_{radial}}{Q_{axial,sup}} \qquad (32)$$

$$\boldsymbol{Q_{axial,inf}} = \boldsymbol{Q_{axial,sup}} \times \mathbf{e}^{\left(\left[-4\times K\times\frac{\mu_S\times d_{Ri}+\mu_{SB}\times d_{Re}}{d_{Re}^2-d_{Ri}^2}\right]\right)} \times \boldsymbol{e_P} \qquad (33)$$

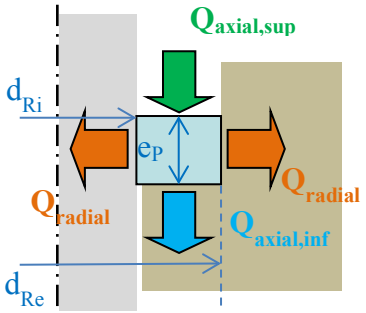

Figure 15: K and μ_{SB} definition

The test sequence for protocol1 is:

1. Application of initial stress, Q_{A1}, on the packing upper face
2. Application of stem movement (linear or rotation) for stress homogenization within the packing stack while maintaining Q_{A1}, at ambient temperature T_{amb}
3. Heating (ramp 2°C/min) to the desired temperature T with a stabilization phase of 4 hours at T while maintaining Q_{A1} (to get the characteristics after creep)
4. Application of the axial stress $Q \leq Q_{A1}$
5. Application of 10 stem movements while maintaining the load at Q
6. Resume from 4 to 5 with new values of Q (less than the previous one)
7. Resume from 1 with $Q_{A2} \geq Q_{A1}$

4.2.2.2 Test Protocol2

The second mechanical test protocol aims to determine the following characteristics:

- The rigidity of the packing when they are unloaded as a modulus of elasticity. This module is used to calculate the force variation associated to the variation of the available height for the packing between the initial tightening situation and the considered service condition.
- The packing coefficient for creep or relaxation.

The test sequence involved in Protocol2 is:

1. Application of stress Q, on the upper face ring
2. Application of stem movement (linear or rotation), for stress homogenization within the packing stack, while maintaining Q at ambient temperature T_{amb}
3. Heating (ramp 2°C/min) to the desired temperature T with a stabilization phase of 4 hours at T while maintaining Q (or the packing thickness) for the measurement of creep (or relaxation)
7. Application of the axial stress Q
8. Unload the packing to Q / 3
9. Application of the axial stress Q
10. Natural cooling to ambient temperature, T_{amb}, maintaining stress Q
11. Unloading at Q = 0

4.3 TESTS RESULTS EXAMPLE

4.3.1 Sealing tests results examples

4.3.1.1 Tested Configurations

A series of 14 tests was carried out on stacks of 4 rings, varying the following parameters:

- 2 types of packing material:
  - die-formed graphite ring (industrial graphite foil with a C-content of > 98 % and 1.5 g/cm³ density)
  - braided PTFE
- Type of stem movement: linear or rotation
- Initial contact pressure level
- Helium pressure level

4.3.1.2 Results analysis

Figure 16 shows a test curve example for graphite ring stack with a linear stem movement, 80 MPa initial contact pressure and 10 bar helium pressure. The leakage levels obtained at the end of each 2-hour stabilization stress platens (red circles) are recorded in order to establish a leakage diagram linking the leakage level to the contact pressure level applied by the gland on the upper face of the packing, as shown in Figure 17. Leakage rates are expressed in mg/s/m of stem perimeter for coherence with the sealing classes (AH, BH, CH) defined in [4]. The intersections of the leakage curve with the sealing classes gives the minimum residual contact pressure levels required to reach the different tightness classes presented in table form in Figure 17.

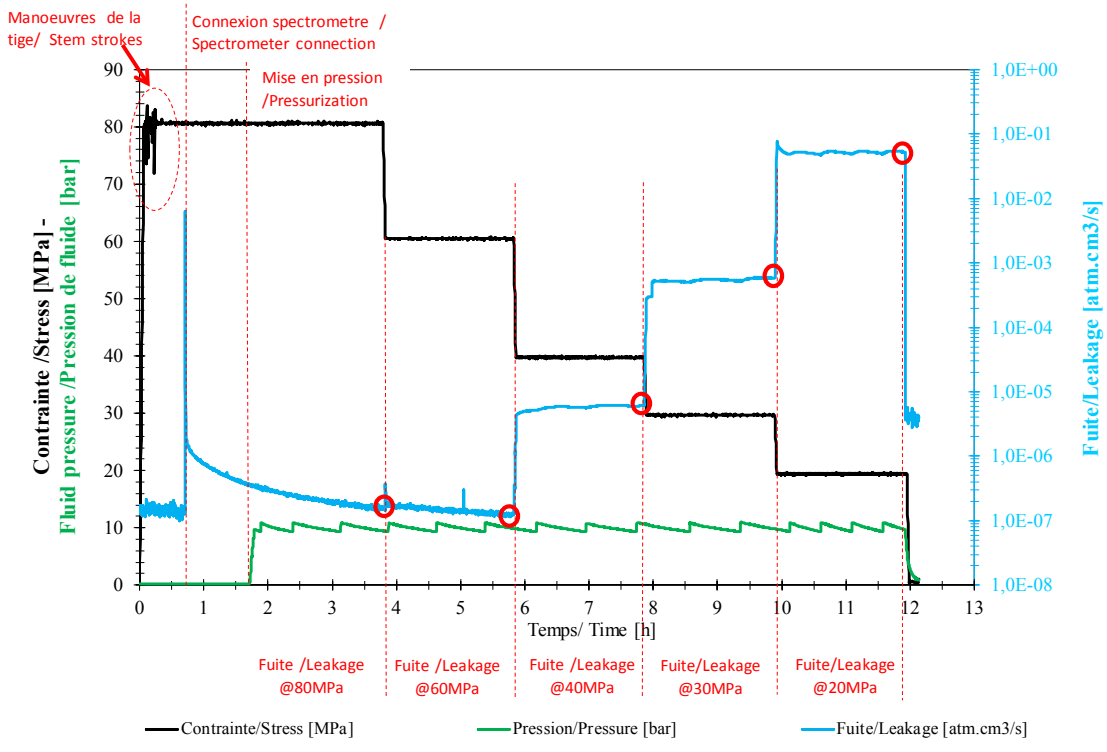

Figure 16: Sealing test measurement example (graphite packing)

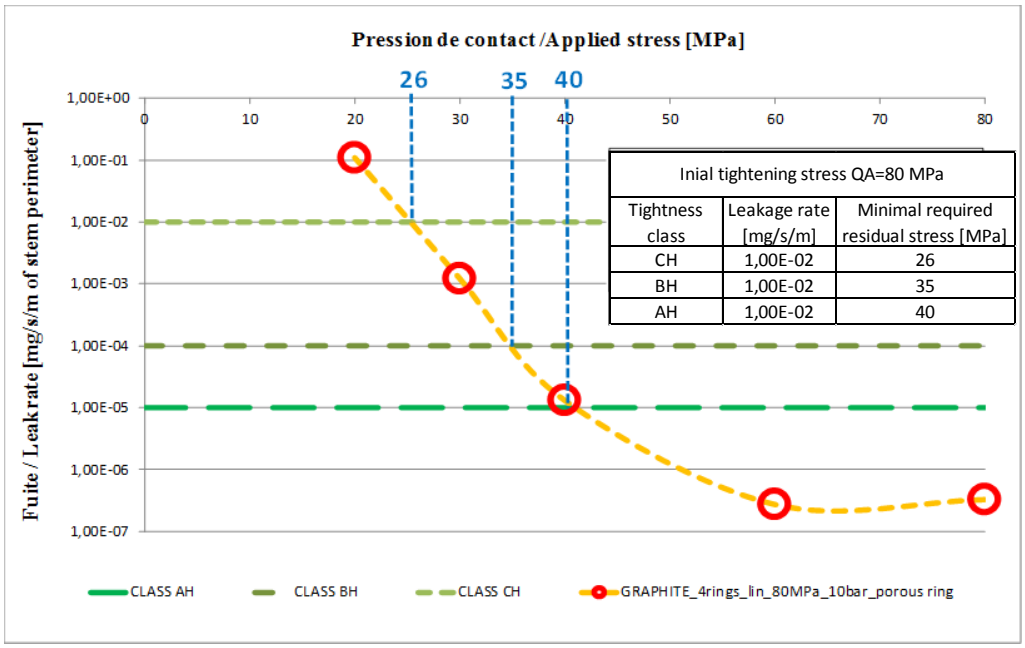

Inial tightening stress QA=80 MPa		
Tightness class	Leakage rate [mg/s/m]	Minimal required residual stress [MPa]
CH	1,00E-02	26
BH	1,00E-02	35
AH	1,00E-02	40

Figure 17: Sealing diagram and table example (graphite packing)

In a similar manner, a diagram obtained for PTFE braided packing with rotating (1/4 turn) stem movements for two initial contact pressure levels (20 and 40 MPa) and two fluid pressure levels (10 and 40 bar) is shown in Figure 18. From this diagram, Table 2 can be defined. This table shows that for a pressure of 10 bar, the sealing classes AH and BH cannot be obtained with an initial clamping of 20 MPa (third column), but that these levels are obtained (with a residual stress of less than 10 MPa) as soon as the initial clamping level reaches 40 MPa (fourth column). The important impact of the initial tightening level on the sealing performance in service is illustrated here. The fifth column shows that for an internal pressure of 40 bar, the initial clamping at 40 MPa makes it possible to ensure a sealing class AH as long as the residual contact pressure is greater than 17 MPa.

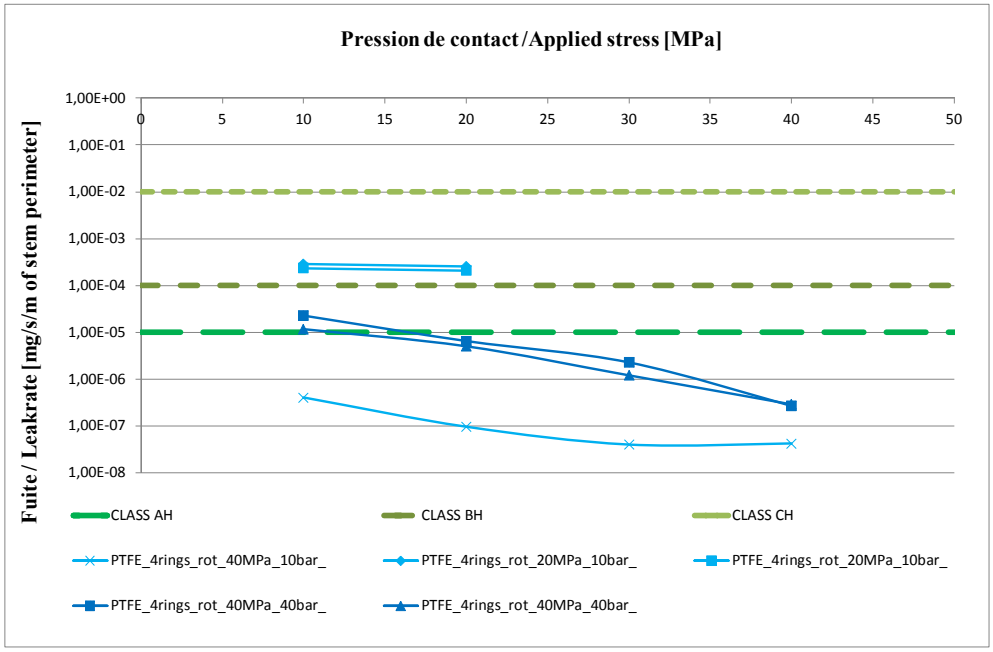

Figure 18: Sealing diagram example (PTFE braided packing)

Table 2: Sealing parameters table example (PTFE braided packing)

Fluid pressure [bar]		10	10	40
Initial stress Q_{A1} [MPa]		20	40	40
Tightness class	Leakage rate [mg/s/m]	Minimal required residual stress [MPa]		
CH	1.00E-02	<10	<10	<10
BH	1.00E-04		<10	<10
AH	1.00E-05		<10	17

4.3.2 Mechanical tests results examples

4.3.2.1 Tested configurations

A series of 12 tests was performed (rotation type stem movements) with following parameters:

- 2 types of packing material:
  - die-formed graphite ring (industrial graphite foil with a C-content of > 98 % and 1.5 g/cm³ density)
  - braided PTFE
- Number of rings: 1 to 3
- Initial contact pressure level

- Test protocol: protocol1 or protocol2

4.3.2.2 *Analysis of results according to protocol1*

The various parameters are continuously recorded over the test duration (Figure 19). Then, a specific data treatment allows extracting the test sequence key points (Figure 20).

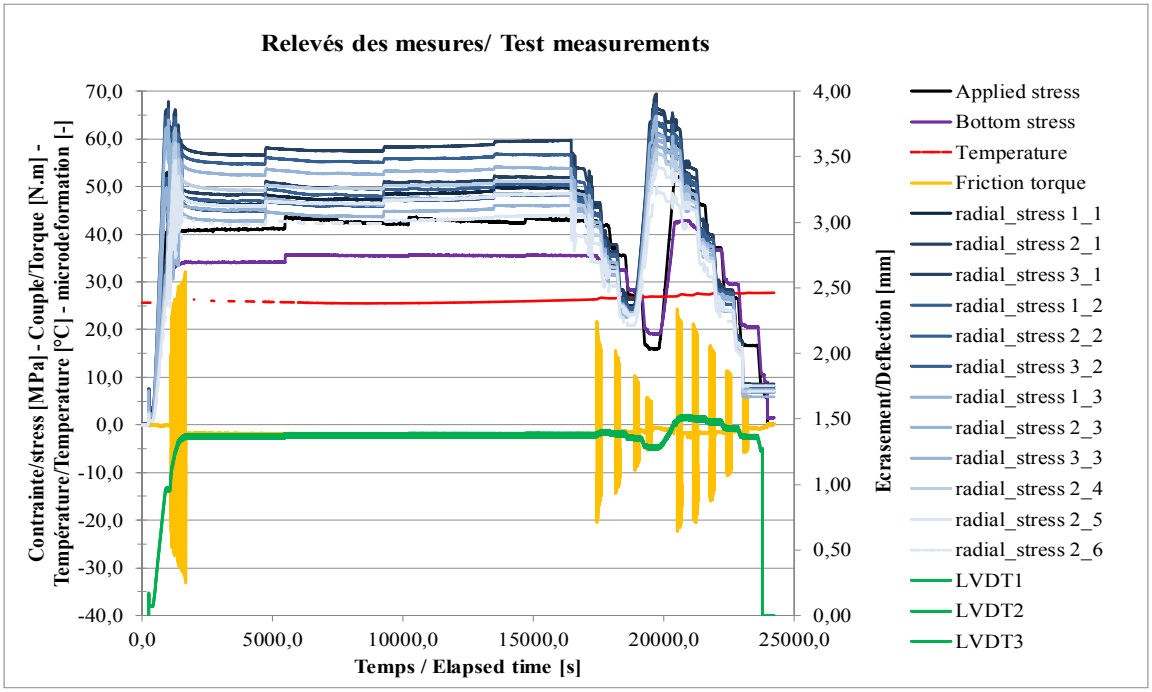

Figure 19: Test protocol_1 measurements example

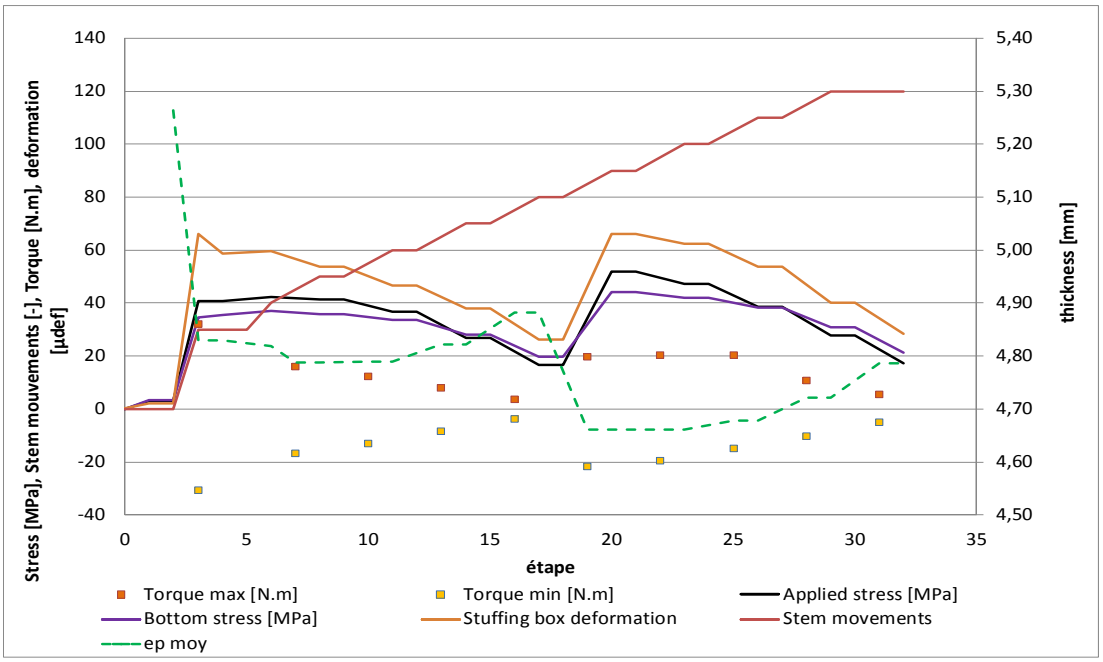

Figure 20: Test protocol_1 analyzed data example

4.3.2.2.1 Packing deflection

Figure 21 gives an example of the deflection measurement obtained from the reading of the three displacement transducers positioned at 120 ° around the test cell. This test was carried out on a single graphite ring. There is a very small difference between the signals of the three sensors (less than 0.05 mm for an average deflection around 1.5mm) demonstrating a good axi-symmetry of assembly force application. A deflection of approximately 1 mm under a contact pressure of 40 MPa for the tested ring with an initial thickness of 6.35 mm corresponds to a deformation of 1 / 6.35 = 16% consistent with the measurements carried out in [5]. Similarly, testing on a stack of 3 rings of the same type showed a slightly lower overall deformation level (around 11% under 40 MPa) due to the interaction between the rings, in coherence with the measurements of [5]. Tests carried out on 1, 2 and 3 PTFE rings showed identical trends but with higher deformation levels.

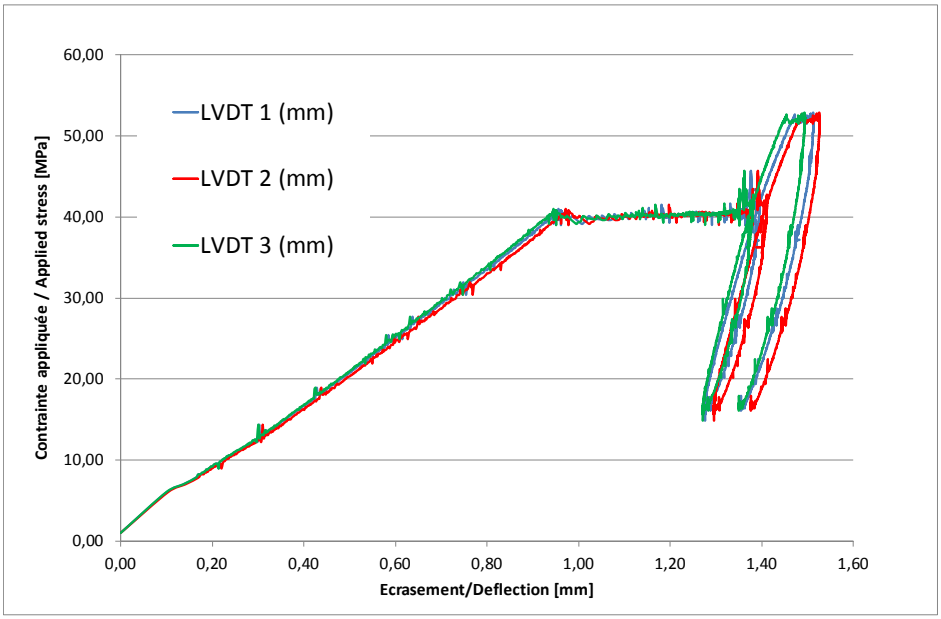

Figure 21: Deflection curve example on one graphite ring

4.3.2.2.2 Axial-> radial transmission of forces (lateral parameter K)

Table 3 shows the evolution of parameter K with the decrease of the axial stress applied by the gland, for two levels of initial axial stresses (40 and 50 MPa) on a graphite ring. A higher K value is observed for 50 MPa initial stress level than for 40 MPa. This reflects the densification of the material with higher initial compression. On the other hand, for a given initial stress (for example 40MPa), an increase in K is observed with the decrease of the stress applied on the upper face of the packing. Values greater than 1 can even be observed. This phenomenon is due to the static friction at stem/packing/housing interfaces, which involves a lower stress decrease on the lower face than on the upper face of the ring during the unloading phase. For the lowest stress levels, there is even a greater stress on the lower face than on the upper face as shown in Figure 20.

For information, a coefficient K' is presented on the right side of Table 3. This parameter uses the average of the axial stresses on the lower and upper faces of the ring as reference instead of the axial stress on the upper face only (see (EQ.1)). This shows stable values of K' during the unloading phase. The introduction of the coefficient K 'for the modeling of the behavior of the packing in the service phases seems therefore more adapted. Table 4 gives the values of K 'for the measurements carried out on braided a PTFE ring. Values lower than those obtained with the graphite rings are naturally observed. An overall stability of K' values are also observed during the unloading phase. K' could be integrated in the calculation method.

Table 3: K and K' results (graphite ring)

		$K= Q_{rad}/Q_{axial,sup}$		$K'= 2*Q_{rad}/(Q_{axial,sup}+Q_{axial,inf})$	
	Q_{A1} [MPa]	40	50	40	50
Q [MPa]	50		0,84		0,90
	40	0,80	0,88	0,86	0,91
	30	0,86	0,93	0,86	0,90
	20	0,95	1,01	0,85	0,92

Table 4: K' results on braided PTFE

	K' [-]	$K'= 2*Q_{rad}/(Q_{axial,sup}+Q_{axial,inf})$	
	Q_{A1} [MPa]	20	30
Q [MPa]	30		0,69
	20	0,67	0,69
	10	0,73	0,72

4.3.2.2.3 Static friction packing/stuffing box (μ_S and μ_{SB})

The calculation method allows taking into account different values of static friction coefficient on the stem side (μ_S) and on the stuffing-box side (μ_{SB}). However, from an experimental point of view it is difficult to measure these values in a differentiated way (particularly on the stem/packing interface). Thus $\mu_S = \mu_{SB}$ is considered as a first approach.

Table 5 gives the μ_{SB} values calculated from the results of tests carried out on graphite and braided PTFE rings. As mentioned above, during the unloading phases, the contact pressure on the lower face of the ring can be greater than on the upper face, resulting in negative values of the μ_{SB} coefficient. Even though this value has no real physical meaning as friction coefficient, it remains valid to determine the stress transmission between the upper and lower faces of the rings in the calculations under unloading. Coefficient μ'SB associated to K' could also be introduced in the calculation method.

Table 5: Values of μSB

Graphite ring				Braided PTFE			
		μ_{SB} [-]				μ_{SB} [-]	
	Q_{A1} [MPa]	40	50		Q_{A1} [MPa]	20	30
Q [MPa]	50		0,13	Q [MPa]	30		0,09
	40	0,12	-0,02		20	0,07	-0,06
	30	0,01	-0,06		10	-0,11	-0,15
	20	-0,09	-0,12				

4.3.2.2.4 Dynamic friction coefficient at stem/packing interface (μ_{f_rot})

The measurement of the friction torque during the stem movements (see Figure 19 and Figure 20) enables to calculate the friction coefficient for rotation according to the equation (34). A similar calculation enables to determine the friction coefficient for linear stem movements from the forces measured during the test.

$$\mu_{f\_rot} = \frac{T_f \times 2/d_S}{\left(\frac{Q_{axial,sup} + Q_{axial,inf}}{2}\right) \times \pi \times K \times d_S \times e_P} \qquad (34)$$

Table 6 shows the results obtained for the two types of packing. For the PTFE braided packing, values are globally lower for the initial clamping levels and more stables with the packing unloading compared with the graphite rings. It must be noticed here that the PTFE braided ring greater deflection can involve greater μ_{f_rot} than for graphite ring even if the measured torque T_f is lower.

Table 6: Dynamic friction coefficient at stem/packing interface values (μf_rot)

	Graphite packing				Braided PTFE		
		μ_{f_rot} [-]				μ_{f_rot} [-]	
	Q_{A1} [MPa]	40	50		Q_{A1} [MPa]	20	30
Q [MPa]	50		0,13	Q [MPa]	30		0,10
	40	0,13	0,12		20	0,12	0,11
	30	0,10	0,10		10	0,12	0,11
	20	0,08	0,07				

4.3.2.3 Analysis of results according to test protocol2

As part of the first ambient temperature test, the analysis focused on the elastic modulus during packing unloading. Future tests will also investigate the creep/relaxation behavior relaxation.

4.3.2.3.1 Ring unloading elastic modulus (E_R)

This coefficient is determined on the basis of the ring thickness increase under unloading to 1/3 of the initial applied stress. This analysis follows the method developed for gaskets in the test protocol [6]. Table 7 shows similar values for the various tests carried out on the graphite rings. For braided PTFE, the tests show a stiffening (modulus multiplied by 1.2) with initial compression increase from 20 to 40 MPa

Table 7: Ring unloading elastic modulus (E_R) measured values

type bague	mouvement	contrainte initiale [MPa]	E_R [MPa]
graphite	rotation	40	1190
graphite	rotation	40	1282
graphite	rotation	60	1128
graphite	rotation	60	1150
PTFE	rotation	40	1220
PTFE	rotation	20	1008

5 APPLICATION EXAMPLE

5.1 Test case definition

5.1.1 Geometry

5.1.1.1 Packing configuration

- n : nombre de bagues dans l'empilement : n = 6 bagues
- k_{seal} : Plus grande valeur de k pour laquelle la fonction d'étanchéité est requise : kseal = 5 (prise en compte anti-extrusion en fond de packing)
- d_{Ri}, d_{Re} : diamètres interne (tige) et externe (boîtier) des garnitures (considérés identiques pour toutes les garnitures de l'empilement et dans toutes les situations)dRi = 25.4 mm (diamètre tige), dRe = 38.1 mm = 25.4 + 2*6.35mm

5.1.1.2 Gland

- d_5 : diamètre réel du trou de boulon = 13.5 mm d'après plan 47498
- d_{Ge} : diamètre extérieur fouloir (pris égal à 72 mm d'après plan 72829)
- d_{GFe} : dimension extérieure de la bride ovale dans la section avec trou de boulon = 95 + 2*14 = 123 mm (d'après plan 47498)
- d_{GFe}' : dimension extérieure de la bride ovale dans la section sans trou de boulon = 27*2 = 54 mm (d'après 47498)
- d_{GFi} : diamètre intérieur de la bride de fouloir = 29.5 mm (d'après 47498)
- e_{GF} : épaisseur du plateau de la bride du fouloir = 25 mm (18mm selon les plans mais porté à 25mm pour obtention taux de charge inférieur à 100% dans l'étude de sensibilité)
- b : double largeur calculée de portée de la bride = d_{GFe} - d_{GFi} – 2*d_5 = 123 - 29.5 – 2*13.5 = 66.5 mm
- l_G : longeur du fouloir en contact avec la boulonnerie et celle en contact avec la première bague = 32 mm (d'après plan 71879 – en première approche sans calcul au niveau des chanfreins)

5.1.1.3 Définition du boitierStuffing box

- e_{SB} : épaisseur du plateau de bride du boîtier = 12 mm d'après plan 97103 (approche conservative)
- l_{SB}: distance axiale entre le fond et la face supérieure du boîtier (pris tel que le fouloir soit engagé sur 10mm avant compression soit 10 + 6*6.35) = 48.1 mm
- d_{ISB} : diamètre interne du boitier=38.2 mm
- d_{ESB} : diamètre externe du boitier=64 mm (d'après plan 97103 et rapport de propotionalité avec autre côte sur plan)

5.1.1.4 Stem

- d_S : diamètre de la tige = 25.4 mm

5.1.1.5 Bolting

- n_B : nombre de boulons = 2
- d_3 : diamètre du cercle de boulonnage = 95 mm (plan 47948)
- d_B : diamètre du boulon = 12 mm (mesure)

5.1.2 *Operating conditions*

- serrage
- mise en pression à température ambiante 40 bar
- chauffe à 200°C avec p interne à 40 bar

5.1.3 *Metallic material parameter*

5.1.3.1 Material data

Le robinet est constitué des matériaux métalliques suivant :

- Tiges filetées ASTM A193 B7 (source [9])
- Ecrous : ASTM A194 Grade 2H (source [9]) - non utilisé dans calcul analytique
- Fouloir : ASTM A216 Gr WCB
- Bride de fouloir : A105
- Tige : ASTM A182 grade F6a (source [9]) - (1.4006) – propriétés mécaniques selon [13] – non utilisé dans calcul analytique
- Chapeau/boitier : ASTM A216 Gr WCB (groupe 2.2)

Table 8: Propriétés des matériaux constitutifs du robinet (configuration 1)

	$R_m t$ [MPa]					
Température [°C]	20	100	150	200	250	300
A193 B7	860	860	860	860	860	860
ASTM A216 Gr WCB	485	485	485	485	485	485
A105	485	485	485	485	485	485
	$R_p 0.2t$ [MPa]					
Température [°C]	20	100	150	200	250	300
A193 B7	720	671	648	632	614	595
ASTM A216 Gr WCB	250	227	219	213	204	194
A105	250	227	219	213	204	194
	Alpha (X 1 E6) [$°C^{-1}$]					
Température [°C]	20	100	150	200	250	300
A193 B7	10.9	11.5	11.9	12.3	12.6	12.9
ASTM A216 Gr WCB	10.9	11.5	11.9	12.3	12.6	12.9
A105	11.5	12.1	12.4	12.8	13.1	13.2

5.1.3.2 Design stresses

- Boulonnerie (règle du §11.4.3.1 de EN 13445-3 V1 [14]) : « *pour les aciers au carbone et les autres aciers non austénitiques, la plus petite des valeurs suivantes : Rp0,2/3 mesurée à la température de conception ou Rm/4 mesuré à température ambiante*

Table 9: Contraintes nominales de calcul pour la boulonnerie

	fB [MPa]					
Température [°C]	20	100	150	200	250	300
A193 B7	215	215	215	210	204	198

- Bride de fouloir (règle du tableau 6.1 source [14]), pour acier autre que austénitique selon §6.2. en condition normale de service :

$$f_d = \min\left(\frac{R_{p0,2/T}}{1,5}; \frac{R_{m/20}}{2,4}\right)$$

Table 10: Contraintes nominales de calcul pour la bride de fouloir

	fG [MPa]					
Température [°C]	20	100	150	200	250	300
A105	166	151	146	142	136	129

- Boitier (règle du tableau 6.1 de EN 13445-3 V1 - source [14]), pour aciers moulés selon §6.6 en condition normale de service :

$$f_d = \min\left(\frac{R_{p0,2/T}}{1,9}; \frac{R_{m/20}}{3}\right)$$

Table 11: Contraintes nominales de calcul pour le boitier

	fG [MPa]					
Température [°C]	20	100	150	200	250	300
ASTM A216 Gr WCB	131	119	115	112	107	102

5.1.3.3 *Packing material parameters*

Include packing material datasheet from performed test here for graphite Ring & braided PTFE

5.1.4 *Tightening*

- Pas de dispersion de serrage

5.1.5 *Live loading*

- Pas de système de live-loading dans un premier temps

5.1.6 *Sum up of calculation parameters*

geometry

garniture/packing		
n	7	
k_{seal}	7	n°
d_{Ri}	25,4	mm
d_{Re}	38,1	mm
lp	44,45	mm
epaiseur libre/ uncompressed thickness		
eP0,1	6,35	mm
eP0,2	6,35	mm
eP0,3	6,35	mm
eP0,4	6,35	mm
eP0,5	6,35	mm
eP0,6	6,35	mm
eP0,7	6,35	mm

fouloir/gland		
lG	32	mm
d_{Ge}	42	mm
d5	13,5	mm
d_{GFe}	123	mm
d_{GFi}	29,5	mm
eGF	25	mm

boitier/stuffing box		
e_{SB}	12	mm
l_{SB}	48,1	mm
d_{iSB}	38,2	mm
d_{ESB}	64	mm

tige/stem		
d_S	25,4	mm

boulonnerie/bolt		
nB (>1)	4	
d3	95	mm
dB	12	mm
lB	70,35	mm
l_{LL}	5	mm
AB	452	mm2

Serrage / tightening

Live Loading oui

Situation	0	1	2	3
K_{LL} [N/mm]		5,00E+02	5,00E+02	5,00E+02
F_{LLmax} [N]		3,20E+04	3,20E+04	3,20E+04
epsi-	0,2			
epsi+	0,2			

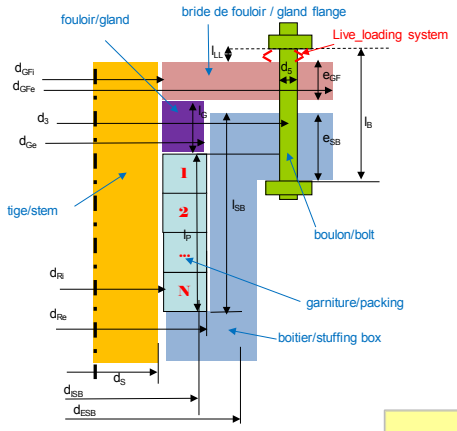

Using conditions & Material data

Température & Pression/Temperature & Pressure

Situation	0	1	2	3
TP[°C]	20	20	200	400
TG [°C]		20	200	300
TGF [°C]		20	200	300
TSB [°C]		20	200	300
TB [°C]		20	200	300
P [MPa]		6	4	5
Q_A [MPa]	40			
Q_{smin} [MPa]		25	30	20

Coefficients de dilatation/Thermal expansion

Situation	0	1	2	3
αG [K^{-1}]		1,09E-05	1,10E-05	1,23E-05
αGF [K^{-1}]		1,09E-05	1,10E-05	1,23E-05
αSB [K^{-1}]		1,15E-05	1,22E-05	1,28E-05
αB [K^{-1}]		1,33E-05	1,33E-05	1,33E-05

contraintes nominales/nominal stress

Situation	0	1	2	3
fB [MPa]	215	215	210	210
fG [MPa]	166	166	142	142
fSB [MPa]	131	131	112	112
maximum friction force [N]	100000	100000	100000	100000
movement type	translation			

ONLY LIGHT YELLOW CELLS HAVE TO BE FILLED

CALCULATE

Input data should be filled up in "user interface" and "packing data" sheets (light yellow cells) before starting calculation using

Developped on Excel 2010. Use "," for decimal separator.

5.2 Results & analysis

5.2.1 *Nominal test case*

Results

FB0,allreq	3,98E+04	N
FB0min	3,98E+04	N
FB0nom	4,98E+04	N
FB0max	5,97E+04	N

Situation		0	1	2	3
FB0,Ireq	N	3,98E+04	2,91E+04	3,25E+04	2,07E+04
ΔFTreq	N		0,00E+00	8,81E+02	4,28E+02
ΔFTmax	N		0,00E+00	1,35E+04	3,03E+04
ΔFMreq	N		-4,57E+02	-6,57E+02	-7,04E+02
ΔFMmax	N		-1,49E+04	-1,83E+04	-2,25E+04
FQ	N		3,80E+03	2,53E+03	3,17E+03
FBI,Ireq	N	3,98E+04	2,86E+04	3,27E+04	2,04E+04
FBImax	N	5,97E+04	4,48E+04	5,49E+04	6,76E+04
FPreq	N		2,48E+04	3,02E+04	1,73E+04
FPmax	N		4,86E+04	5,74E+04	7,07E+04
$F_{friction\_max}$	N	2,27E+04	1,85E+04	2,18E+04	2,68E+04
ϕB	%	61%	46%	58%	71%
ϕG	%	21%	16%	23%	28%
ϕSB	%	98%	80%	110%	136%
ϕfriction	%	23%	18%	22%	27%

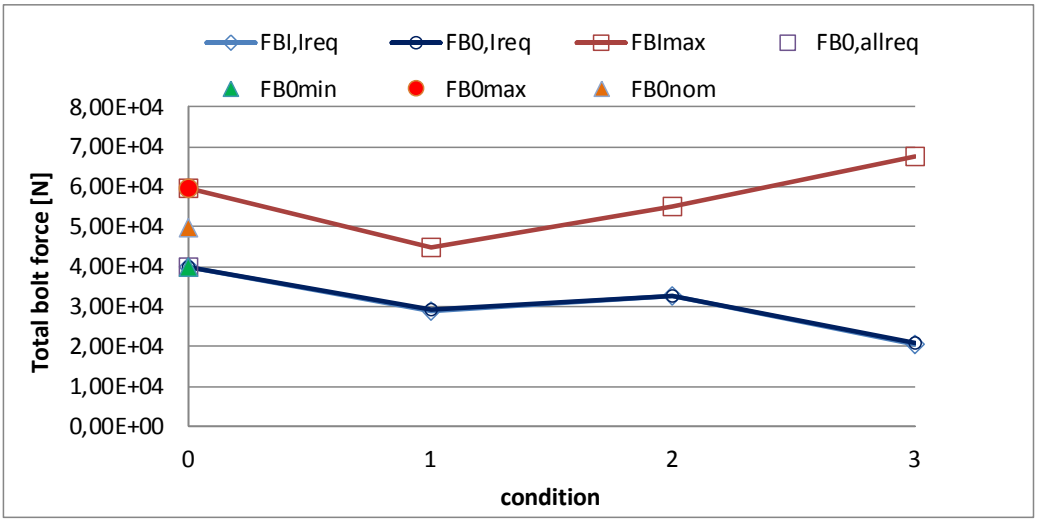

+ Graphs to be added

5.2.2 Nominal test case + tightening dispersion

5.2.3 Nominal test case + live-loading system

5.2.4 Nominal test case + dispersion on packing parameters

cas			FB0allreq	ΦB_0	ΦB_1	ΦB_2	ΦGF_0	ΦGF_1	ΦGF_2	ΦSB_0	ΦSB_1	ΦSB_2	Φfriction_0	Φfriction_1	Φfriction_2
1	µS	0.5	100%	100%	100%	100%	100%	100%	100%	100%	100%	100%	100%	100%	100%
3	µS	1.5	94%	94%	94%	95%	94%	94%	95%	94%	95%	95%	98%	99%	99%
4	µSB	0.5	106%	106%	106%	106%	106%	106%	106%	106%	106%	105%	102%	102%	101%
6	µSB	1.5	91%	91%	91%	92%	91%	91%	92%	91%	92%	93%	97%	98%	99%
7	K	0.5	110%	110%	110%	109%	110%	110%	109%	110%	109%	108%	103%	102%	102%
9	K	1.5	86%	86%	86%	87%	86%	86%	87%	43%	43%	44%	48%	48%	49%
10	ep	0.5	102%	102%	102%	102%	102%	102%	102%	106%	106%	106%	105%	105%	106%
12	ep	1.5	86%	86%	86%	87%	86%	86%	87%	86%	87%	88%	48%	48%	49%
13	Ep	0.5	116%	116%	116%	115%	116%	116%	115%	116%	115%	114%	158%	156%	154%
15	Ep	2	100%	100%	100%	100%	100%	100%	100%	100%	100%	100%	100%	100%	100%
16	Rx	0.5	100%	100%	100%	100%	100%	100%	100%	100%	100%	100%	100%	100%	100%
18	Rx	1.5	200%	200%	100%	100%	200%	100%	100%	200%	100%	100%	200%	100%	100%
19	µf	0.5	88%	88%	97%	120%	88%	97%	120%	88%	98%	119%	88%	98%	116%
21	µf	1.5	100%	100%	100%	100%	100%	100%	100%	100%	100%	100%	50%	50%	50%
22	alphaP	0.5	100%	100%	100%	100%	100%	100%	100%	100%	100%	100%	150%	150%	150%
24	alphaP	1.5	100%	100%	100%	100%	100%	100%	100%	100%	100%	100%	100%	100%	100%
28	QA	0.5	100%	100%	100%	100%	100%	100%	100%	100%	100%	100%	100%	100%	100%
30	QA	1.5	100%	100%	100%	100%	100%	100%	100%	100%	100%	100%	100%	100%	100%
31	Qsmin	0.5	132%	132%	132%	124%	132%	132%	124%	132%	129%	122%	132%	129%	119%
33	Qsmin	1.5	88%	88%	88%	90%	88%	88%	90%	88%	89%	91%	88%	89%	93%

6 REFERENCES

[1]: EN1591-1: Flanges and their joints - Design rules for gasketed circular flange connections - Part 1: Calculation method, 2013

[2]: EN13555: Flanges and their joints - Gasket parameters and test procedures relevant to the design rules for gasketed circular flange connections, 2014

[3]: EN1591-4: Flanges and their joints - Part 4: Qualification of personnel competency in the assembly of bolted connections of critical service pressurized systems, 2013

[4] VDI 2440, Emission control – Mineral oil refineries, 2000

[5] API 622, Type testing of process valve packing for fugitive emissions, 2011

[6] ISO 15848-1, Industrial valves - Measurement, test and qualification procedures for fugitive emissions - Part 1: Classification system and qualification procedures for type testing of valves, 2006

[7] API 624, Type Testing of Rising Stem Valves Equipped with Graphite Packing for Fugitive Emissions, First Edition, 2014

[8] Nowak, H, 1998, "Guide pratique pour la mise en oeuvre correcte des presse-garniture de la robinetterie des centrales nucléaires et thermiques à flamme", EDF-DER, Nov. 1998

[9], Société Nouvelle de Robinetterie Industrielle, "Robinetterie Industrielle", 1992.

[10] FSA & ESA, 2008, “Guidelines for the Use of Compression Packings”, prepared by Fluid Sealing Association and European Sealing Association, Technical Manual, 3rd Edition, 2008

[11] CETIM, Sauger et al, 2003, E. Sauger, A. Naidon, T. Ledauphin, Y. Birembaut, « Outil de dimensionnement des étanchéités de tige de manœuvre. étanchéités de garniture », rapport étude interne n°1D1250, 2003.

[12] Sauger et al, Etude des paramètres hauteur/Course/diamètre sur les garnitures graphite et PTFE rapport CETIM n° 1K1892, 2005

[13] Ruaidhe and Torrance, “Stress analysis and durability of valve packing Rings”, Department of Mechanical and Manufacturing Engineering, Trinity College Dublin, 2003

[14] M. Diany and A.-H. Bouzid, “Short Term Relaxation of Stuffing Box Packings”, PVP, San Antonio, Texas, USA, 2007

[15] Diany and Bouzid, “Analytical Evaluation of Stresses and Displacements of stuffing box packing based on a flexibility analysis”, Triblogy International, Vol.42, pp. 980-986, 2009

[16] S. Ciortan & I. Birsan: Advanced Investigation method for stuffing box packings functioning, The annals of University “Dunarea de Jos”, Fasicle VIII, Tribology, Romania, 2002, pp. 91-93, 2002

[17] H.K. Müller, B. S. Nau, « Fluid Sealing Technology, Principles and Applications », ISBN:0-8247-9969-0,Chapitre 11, Compression Packings, pp. 199-214, 1998

[18] Klenk et al : Kennwerte fur Stopfbuchspackungen, MPA Stuttgart, 1999

[19] Diany and Bouzid, Creep Constitutive Law of Packing Materials Based on Relaxation Tests, PVP2011-57271 (ASME, Pressure Vessel and Piping conference - Baltimore, USA), 2011

[20] Veiga et al, Valve packings seating stress, 2008 ASME Pressure Vessel and Piping Conference, July 27-31, 2008, Chicago, Illinois, USA, PVP2008-61214, 2008

[21] EN12516-2: Industrial valves- Shell design strength - Part 2: Calculation method for steel valve shells, 2004

[1] H.Lejeune, Y.Ton That (Cetim), “Tool development for design and optimisation of valve packings.” Indutrial Valve Summit, 28/05-2015.

[2] CEN, “NF EN 1591-1: Flanges and their joints - Design rules for gasketed circular flange connections - Part 1: Calculation method.” AFNOR, 2014.

[3] API, “API 622 (2nd_Ed) - Type Testing of Process Valve Packing for Fugitive Emissions.” API, 2011.

[4] AFNOR, “NF EN ISO 15848-1: Industrial valves — Measurement, testand qualification procedures for fugitive emissions —Part 1: Classification system and qualificationprocedures for type testing of valves.” AFNOR, 2015.

[5] Klenk, Th (Staatliche Materialprüfungsanstalt - MPA), “Kennwerte für Stopfbuchspackungen: Abschlußbericht.” .